International Journal of Nanomedicine

Dovepress
Taylor & Francis Group

Open Access Full Text Article

ORIGINAL RESEARCH

Enhanced Sonodynamic Therapy via Au Nanoclusters Deposited on TiO_2 Nanosheets

Lei Huang[1,*], Lineng Wei[2,*], Dan Li[2], Weiqing Zhang[2], Lidong Liu[1]

[1]Department of Medical Imaging Center, Guangxi Medical University Cancer Hospital, Nanning, Guangxi, 530021, People's Republic of China; [2]Department of Experimental Research, Guangxi Medical University Cancer Hospital, Nanning, Guangxi, 530021, People's Republic of China

*These authors contributed equally to this work

Correspondence: Weiqing Zhang; Lidong Liu, Email zhangweiqing@tjut.edu.cn; evanlld@sina.com

Purpose: This study aimed to enhance the efficacy of sonodynamic therapy (SDT) for breast cancer by engineering TiO_2 nanosheets modified with Au nanoclusters (TiO_2-Au), thereby improving reactive oxygen species (ROS) generation under ultrasound (US) irradiation.

Methods: TiO_2-Au sonosensitizers were synthesized via a deposition–precipitation with urea (DPU) method and characterized by TEM, XRD, and XPS. ROS generation efficiency was quantified using DPBF, TMB, and NBT probes, along with electron spin resonance (ESR). In vitro therapeutic performance was assessed in 4T1 breast cancer cells via flow cytometry, Calcein-AM/PI staining, and cell counting kit-8 (CCK-8) assay. In vivo efficacy and biosafety were validated in 4T1 tumor-bearing BALB/c mice through tumor growth monitoring, histological analysis, blood biochemistry, and hemolysis assays.

Results: TiO_2-$Au_{10.5}$ exhibited enhanced electron–hole separation, reduced bandgap (from 3.2 to 2.8 eV), and significantly boosted ROS generation under US irradiation. In vitro, TiO_2-$Au_{10.5}$ combined with US induced a 4.25-fold increase in intracellular ROS and a 4.7-fold higher apoptosis rate compared to TiO_2 + US. In vivo, TiO_2-$Au_{10.5}$ + US achieved a tumor growth inhibition index of 76.9% without significant toxicity, as evidenced by normal blood markers, no hemolysis, and no damage to major organs.

Conclusion: Au nanocluster modification effectively tunes the sonodynamic performance of TiO_2 nanosheets by modulating electron–hole separation and ROS production. Notably, varying the Au content enabled precise regulation of SDT efficacy, with TiO_2-$Au_{10.5}$ achieving optimal therapeutic outcomes. These findings highlight TiO_2-Au as a safe, potent, and composition-tunable sonosensitizer platform for precise and effective cancer therapy.

Keywords: TiO_2 nanosheets, gold nanoclusters, Au content modulation, reactive oxygen species, sonodynamic therapy

Introduction

Cancer remains a prominent cause of worldwide fatality and the conventional treatment methods such as surgery, chemotherapy, and radiation often result in significant adverse effects, drug resistance, and non-specific targeting.[1] Consequently, there is a growing interest in developing more selective, less invasive, and safer treatment modalities.[2,3] Sonodynamic therapy (SDT) holds significant potential as a targeted cancer treatment strategy by utilizing low-intensity focused ultrasound (LIFU) and sonosensitizers to generate cytotoxic reactive oxygen species (ROS) within tumor tissues.[4,5] Sonosensitizers are central to the mechanism and effectiveness of SDT. Upon activation by ultrasound (US), they undergo a sonochemical reaction that generates electron-hole pairs. These pairs subsequently engage in interactions with oxygen molecules present within the tumor microenvironment, resulting in the generation of singlet oxygen ($^1O_2$).[6,7] The accumulation of ROS induces oxidative stress, leading to apoptosis and necrosis in cancer cells.[4,8,9] There is a strong need to enhance the therapeutic effectiveness of SDT by developing more efficient sonosensitizers.

Titanium dioxide (TiO_2) nanoparticles have garnered significant attention in SDT due to their unique physico-chemical properties, biocompatibility, and ability to generate ROS upon ultrasound activation, making them promising candidate for cancer treatment.[10–12] However, one of the main challenges is the relatively low ROS

Received: 8 February 2025
Accepted: 30 April 2025
Published: 14 May 2025

yield observed under standard clinical ultrasound frequencies.[13–15] To overcome this limitation, it is crucial to improve the processes governing electron-hole pair formation and recombination during ultrasound activation.[13,15,16] Noble metals like gold (Au), ruthenium (Ru) and platinum (Pt) have been successfully integrated with TiO_2 to narrow its bandgap, improving electron-hole separation and reducing recombination.[15–19] Furthermore, the incorporation of Au exploits the surface plasmon resonance (SPR) phenomenon, leading to an amplification of the localized electromagnetic field surrounding the TiO_2 nanoparticles. This further enhances ultrasound responsiveness and ROS generation.[20–22] The modification of noble metal on TiO_2 significantly increases ROS production, thereby enhancing the cancer cell-killing efficiency of SDT.[7] However, the high cost and potential biocompatibility concerns associated with noble metals limit their widespread clinical application. Thus, determining the optimal noble metal content to maximize ROS generation while preventing excessive particle aggregation remains a challenge.

In this work, we report for the first time novel Au nanoclusters anchored in varying amounts on TiO_2 nanosheets (denoted as TiO_2-Au) and systematically investigate their performance in SDT for breast cancer treatment (Scheme 1). As anticipated, the band gap of TiO_2 decreases progressively with increasing Au nanocluster content. This phenomenon can be ascribed to the increased separation of electron-hole (e^-/h^+) pairs due to the band gap activation of TiO_2. When the Au content reaches 10.5% (TiO_2-$Au_{10.5}$), the band gap is reduced to 2.8 eV, which is considerably smaller than the pristine TiO_2 (3.2 eV). As a result, TiO_2-$Au_{10.5}$ significantly boosts SDT efficiency with a high ROS quantum yield. Comprehensive in vitro and in vivo tumor model experiments confirm that TiO_2-$Au_{10.5}$ greatly enhances the therapeutic effect of SDT against breast cancer compared to pristine TiO_2. This research highlights a promising sonosensitizer for improving SDT efficiency.

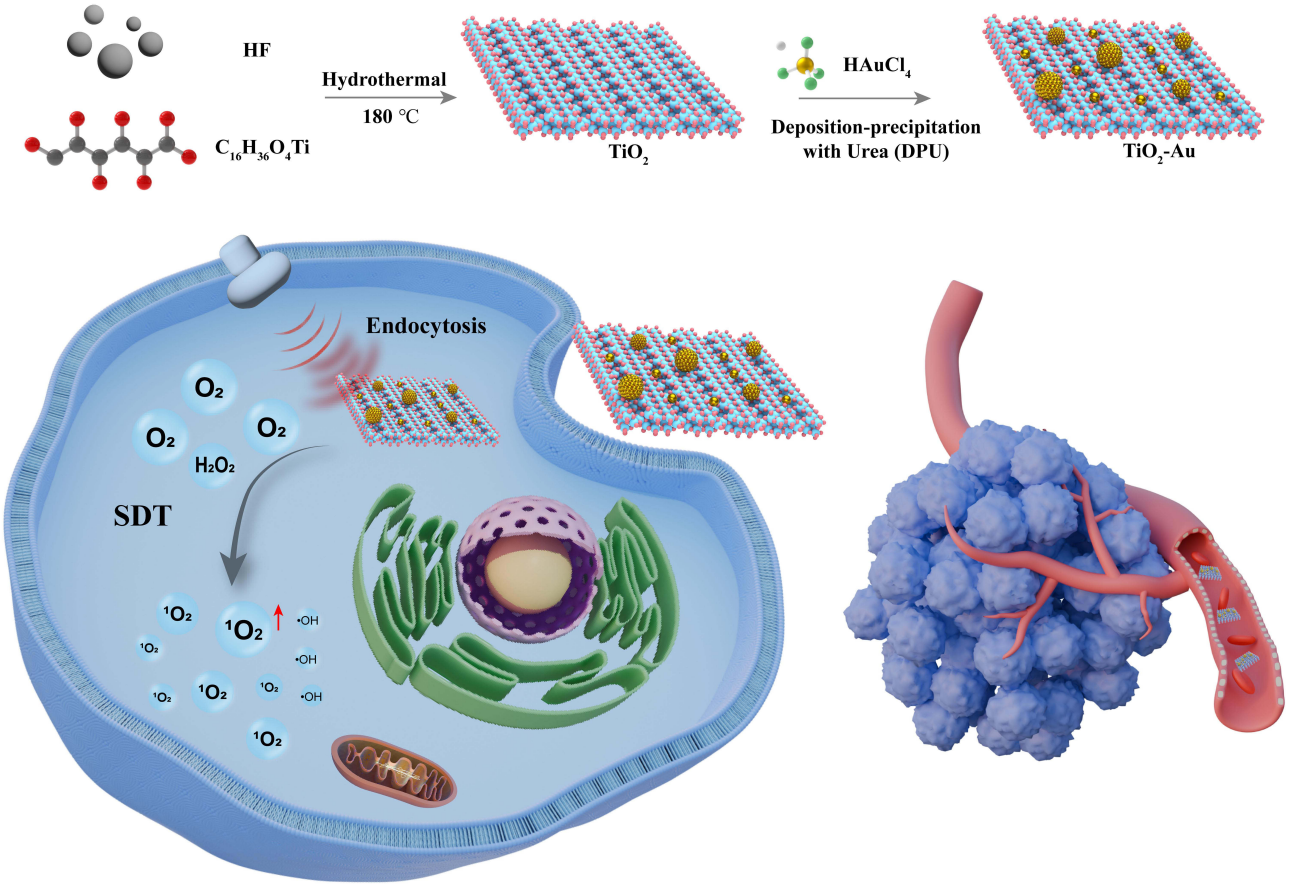

Scheme 1 Schematic illustration of TiO_2-Au for tumor therapy under US exposure.

Materials and Experimental

Materials

All chemicals and reagents were analytical grade and used without any further purification. Tetrabutyl titanate (Ti(OBu)4, Chloroauric acid (HAuCl4) were purchased from Sigma-Aldrich. 1,3-diphenylisobenzofuran (DPBF) was purchased from Macklin (Shanghai, China). 3,3',5,5'-tetramethylbenzidine (TMB) was purchased from Aladdin (Shanghai, China). BBoxiProbe® O28 was purchased from Bestbio (Shanghai, China). Cell counting kit-8 (CCK-8) was provided by Zoman Biotechnology (Beijing, China). NBT, Calcein AM/PI cell double-staining kit, ROS assay kit and Hoest33342 were purchased from Beyotime Biotechnology (Shanghai, China). Annexin V-FITC/PI kit was purchased from Bestbio (Shanghai, China). Fetal bovine serum (FBS), penicillin–streptomycin solution and Dulbecco's Modified Eagle's medium (DMEM) were purchased from Gibco (Shanghai, China). Streptomycin, penicillin, and trypsin were obtained from Solarbio (Beijing, China). The aqueous solution used in the experiment was prepared from deionized water of Milli-Q water purification system.

Experimental

Preparation of TiO_2-Au Sonosensitizers

TiO_2 nanosheets were synthesized using a standard hydrothermal method.[23] Subsequently, Au atoms were deposited onto the TiO_2 substrate via the deposition-precipitation with urea (DPU) process to synthesize the TiO_2-$Au_{10.5}$ sonosensitizers.[17] In brief, a 200 mL of urea solution (0.42 M) containing 0.2 g of TiO_2 nanosheets was mixed with 3 mL of a solution containing $HAuCl_4$ (50 mm) in water. The resulting solution underwent heating and stirring at a temperature of 80 °C for a duration of 14 hours while being shielded from light. Finally, the TiO_2-$Au_{10.5}$ sonosensitizers were thoroughly washed and freeze-dried for further use.

Determination of ROS Generation

The generation of $^1O_2$ in the TiO_2-$Au_{10.5}$-mediated SDT process were detected by using 1,3-diphenylisobenzofuran (DPBF) as probes, respectively. Typically, a certain concentration of probes dissolved in dimethyl sulphoxide (DMSO) was mixed with 200 μg/mL as-synthesized sonosensitizers, which was exposed to US irradiation (1.0 MHz, 50% duty cycle, 1.5 W/cm²) at fixed time intervals in the dark. Then the concentrations of probes were recorded by UV-vis spectra. The generation of hydroxyl radical (•OH) in the TiO_2-Au-mediated SDT process was detected by using 3,3',5,5'-tetramethylbenzidine (TMB) as probes, and the TiO_2-Au (200 μg/mL) was exposed to US irradiation (1.0 MHz, 50% duty cycle, 1.5 W/cm²) for 5 minutes reaction in the dark. Then the concentrations of probes were recorded by UV-vis spectra. The generation of O_2^- in the TiO_2-Au-mediated SDT process was detected by using NBT as probes, and the TiO_2-Au (200 μg/mL) was exposed to US irradiation (1.0 MHz, 50% duty cycle, 1.5 W/cm²) for 5 minutes reaction in the dark. Then the concentrations of probes were recorded by UV-vis spectra. The long-term stability of TiO_2-$Au_{10.5}$ sonosensitizers in physiological environments was assessed by monitoring their optical properties. Freshly prepared TiO_2-$Au_{10.5}$ sonosensitizers were compared with samples stored in PBS and DMEM for one week. Stability was evaluated by measuring the relative absorbance at 412 nm (A_t/A_o) over time using UV-vis spectroscopy.

Intracellular ROS Determination

The 4T1 cell line used in this study was obtained from the ATCC (RRID: CVCL_0125) repository. The total induction of ROS in the 4T1 cells caused by different treatment (Control, US, TiO_2 + US, TiO_2-$Au_{1.3}$ + US, TiO_2-$Au_{6.4}$ + US, and TiO_2-$Au_{10.5}$ + US) was determined by flow cytometer with the sonosensitizer concentration set at 200 μg/mL 4T1 cells were seeded in 24-well plates with a density of 5×10^4 cells overnight for 12 h, depending on the group. Subsequently, cells were stained with DCFH-DA following the manufacturer's instructions according to the manufacturer's instructions. Finally, the cells were digested and flow cytometer was employed for determination. For the BBoxiProbe® O28 staining assay, cells were first stained with Hoest 33342 (5 μg/mL) for 15 min at 37°C to label the nuclei, followed by staining with O28. Fluorescence imaging was then acquired.

Calcein AM/PI Staining and Annexin V-FITC/PI Apoptosis Assay

4T1 cells were subjected to six treatment conditions: Control, US, TiO_2 + US, TiO_2-$Au_{1.3}$ + US, TiO_2-$Au_{6.4}$ + US, and TiO_2-$Au_{10.5}$ + US, with the sonosensitizer concentration set at 200 μg/mL. For the Calcein-AM/PI staining assay, 1 μL of Calcein-AM and 2 μL of PI sequentially added to the treated cells. After staining for 30 minutes, fluorescence images were acquired.

Apoptosis was assessed by staining the cells with FITC-labeled Annexin V and PI, Briefly, cells were resuspended in Annexin V binding buffer, stained with 5 μL of Annexin V-FITC and 5 μL of PI, and incubated for 15 min. The samples were then analyzed by flow cytometry, and apoptotic rates were quantified.

Cell Cytotoxicity Evaluation

The Cell Counting Kit-8 (CCK-8) assay was utilized to evaluate cytotoxicity and cell viability. 4T1 cells were exposed to different concentrations of TiO_2-$Au_{10.5}$ (0, 50, 100, 200, and 300 μg/mL) for a duration of 24 hours. Following rinsing, the treated cells were supplemented with CCK-8 reagent and incubated at a temperature of 37°C for an additional period of 2 hours. The survival rate of the cells was subsequently determined by measuring the optical density (OD) at a wavelength of 450 nm using a microplate reader.

In vivo Antitumor Efficacy Evaluation

Female BALB/c mice weighing around 20 g were used as animal models. All animal experiments were conducted in accordance with the GB/T 35892–2018: Laboratory Animal-Guideline for Ethical Review of Animal Welfare, in addition to obtaining approval from the Ethical Committee of Guangxi Medical University Cancer Hospital (approval number: KY-2022-272). Each mouse was subcutaneously injected with 8×10^5 4T1 cells into their right flank. The tumor-bearing mice were then divided randomly into three groups, each consisting of four mice: Control, US, and TiO_2-$Au_{10.5}$+US. Each group received four intravenous injections of sonosensitizers at a dose of 10 mg/kg. Following the administration, ultrasound (US) irradiation will be applied at a power density of 1.5 W/cm² for a duration of five minutes. Throughout the treatment period, daily records were maintained for body weights and tumor volume. Tumor tissues and major organs were collected for histological analysis using Hematoxylin and Eosin (H&E) staining techniques. Additionally, hematological analysis was performed utilizing a fully automated biochemical analyzer. Blood samples from treated mice were collected over a span of 14 days prior to sacrifice; routine blood tests were promptly conducted while serum separation was achieved through centrifugation at 3000 rpm for a duration of 15 minutes at a temperature of 4 °C in preparation for biochemical analysis.

Hemolysis Assay

Red blood cells (RBC) were obtained from BALB/c mice and diluted with PBS to 2% suspension. TiO_2-$Au_{1.3}$, TiO_2-$Au_{6.4}$, and TiO_2-$Au_{10.5}$ were added to 2% red blood cell suspension to the desired concentrations (25, 50, 100, and 200 μg/mL). It was then incubated at 37 °C for 3 h. An identical red cell suspension incubated with PBS and ultrapure water was used as a negative and positive control under the same conditions. All samples were centrifuged at 3000 rpm for 10 min before accurately absorbing the same volume of the supernatant into a 96-well plate. The hemoglobin release at 540 nm was measured by Varioskan Flash microplate reader.

Statistical Analysis

The statistical significance of experimental data was assessed by employing one-way analysis of variance (ANOVA) with the assistance of GraphPad Prism 9 software. The criteria for determining significance were based on the p-value (P) satisfied the following criteria: *$P < 0.05$, **$0.001 < P < 0.01$, ***$P < 0.001$, while "ns" denoted no significant distinction.

Discussion and Results

As shown in Scheme 1, TiO_2 nanosheets were synthesized using a modified hydrothermal method. The morphology of the as-synthesized TiO_2 was confirmed to be well-defined nanosheets through transmission electron microscopy (TEM) images TiO_2 (Figure S1). Analysis of the lattice spacing revealed distinct lattice fringes measuring 0.19 nm and 0.35 nm,

which correspond to the (200) and the (101) crystal planes of TiO_2, respectively.[24] These TiO_2 nanosheets was employed as supports for Au nanoclusters through the deposition-precipitation with urea (DPU) process to yield TiO_2-Au. By varying the amount of $HAuCl_4$ added (8.5 and 50.9 mg), the Au content on the TiO_2 nanosheets was easily controlled, ranging from 1.3% to 10.5% (Figure 1A–C). Energy dispersive spectroscopy (EDS) elemental mapping of TiO_2-$Au_{10.5}$ confirmed the presence of Ti, O, and Au, verifying the successful deposition of Au on TiO_2 (Figure 1D–G). The average size of the Au nanoclusters was determined to be approximately 1.7 nm. X-ray diffraction (XRD) was employed to examine the crystal structure of TiO_2 prior and following Au deposition (Figure 1H). The observed peaks were attributed to those of anatase-phase TiO_2 (JCPDS no. 21–1272). The XRD patterns of TiO_2-$Au_{1.3}$ and TiO_2-$Au_{6.4}$ exhibited no discernible Au characteristic diffraction peak, probably due to the low loading and ultrafine size of Au nanocluster. When the Au content increased to 10.5%, a subtle Au peak was observed in the TiO_2-$Au_{10.5}$, confirming the presence of Au at higher loading levels. X-ray photoelectron spectroscopy (XPS) analysis confirmed the presence of Au in TiO_2-$Au_{10.5}$ (Figure 1I). Notably, a 0.1 eV blue shift in the Ti 2*p* binding energy following Au modification (Figures 1J and S2–3).[25,26] This shift indicates a partial reduction of Ti^{4+}, suggesting that the Au modification alters the electronic properties of TiO_2. The O 1*s* XPS spectra displayed three characteristic peaks at 529.7 eV, 530.3 eV and 531.6 eV, attributed to O-Ti, vacancy O and O-H bonds, respectively (Figure S4).[27,28] The abundance of Ti-OH groups endowed the TiO_2-Au sonosensitizer with excellent hydrophilicity. In the high-resolution Au 4*f* spectrum, two peaks corresponding to $Au^{\delta+}$ species were observed alongside peaks attributed to Au^0 states, suggesting the coexistence of Au–O sites and metallic Au clusters within the composite (Figure 1K).[28,29]

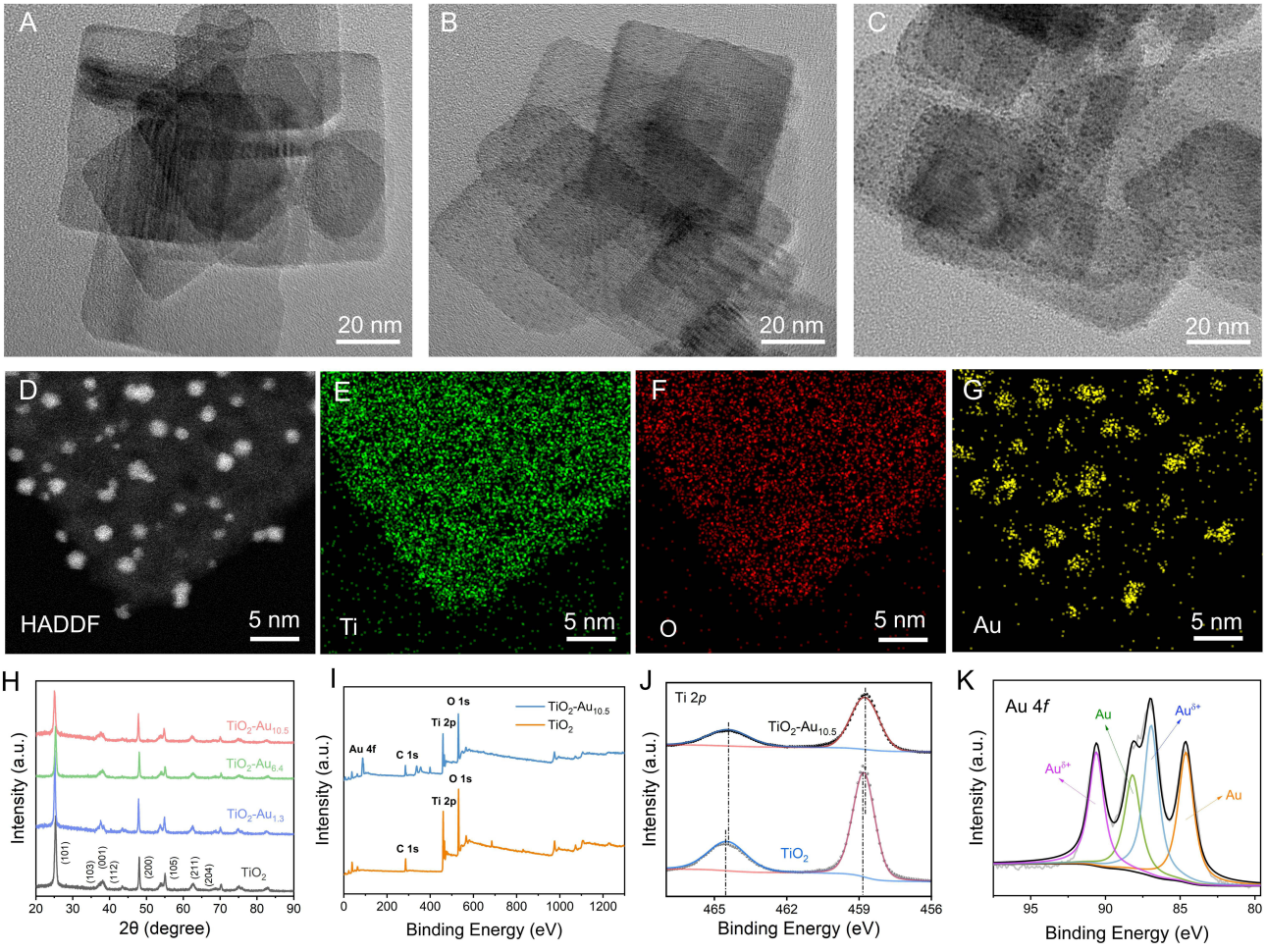

Figure 1 Synthesis and characterizations of Au-TiO_2 sonosensitizer. (**A–C**) TEM image of TiO_2-$Au_{1.3}$, TiO_2-$Au_{6.4}$ and TiO_2-$Au_{10.5}$ sonosensitizer. (**D–G**) EDS mapping images of TiO_2-$Au_{10.5}$. (**H**) XRD pattern of TiO_2 and Au-TiO_2. (**I**) XPS survey spectra of the TiO_2-$Au_{10.5}$, and pure TiO_2. (**J**) XPS characterization of Ti 2*p* for TiO_2-$Au_{10.5}$, and pure TiO_2. (**K**) Au 4*f* high-resolution XPS spectra of TiO_2-$Au_{10.5}$.

https://doi.org/10.2147/IJN.S516314

The generation capacity of $^1O_2$ species was first evaluated using 1,3-diphenylisobenzofuran (DPBF) as a specific sensing probe.[30] The UV-vis spectrophotometer was utilized to track the changes in DPBF absorbance following various treatments. Figures 2A–C illustrates a significant reduction in DPBF absorbance with increased Au loading and extended US irradiation. The intensity was reduced by 50% after treatment with TiO_2-$Au_{10.5}$ under US irradiation for 120 seconds. The rate of DPBF degradation for US-treated TiO_2-Au groups, especially TiO_2-$Au_{10.5}$, was significantly faster than that of the US-treated TiO_2 group (Figure 2D). While $^1O_2$ generation efficiency improves with increasing Au content, the enhancement peaks at 10.5% and begins to decline beyond this point, likely due to excessive Au hindering electron-hole separation. These results indicate that TiO_2-$Au_{10.5}$ achieves an optimal balance between ROS generation and SDT efficiency, outperforming pristine TiO_2 in the sonodynamic process. In addition, electron spin resonance (ESR) measurements were conducted to detect the $^1O_2$ production using 2,2,6,6-tetramethylpiperidine (TEMP) as spin trap reagents. Under US irradiation, TiO_2-Au groups exhibited stronger characteristic TEMP/$^1O_2$ adducts signals compared to pristine TiO_2 (Figure 2E), which is consistent with the findings in the above colorimetric assays. Stability assessments demonstrated that TiO_2-$Au_{10.5}$ nanoparticles maintained excellent structural integrity in physiological environments (PBS and DMEM) over one week, as evidenced by consistent optical absorbance properties (Figure S5). This robust stability ensures the nanoparticles' reliable functionality for subsequent applications in reactive oxygen species (ROS) generation studies.

Hydroxyl radical (•OH) production was evaluated using 3,3′,5,5′-tetramethylbenzidine (TMB) and the specific red fluorescent probe BBoxiProbe® O28. The increase of •OH levels was detected in TiO_2-Au treated by US for 5 minutes (Figures S6-S8). At the same time, nitrotetrazolium blue chloride (NBT) was employed as a probe to investigate the generation of O_2^- by TiO_2-Au. However, no significant increase in absorption values at 595 nm (the absorption peak of the generated compound when O_2^- was produced) was detected following US irradiation (Figure S9). These results indicated that TiO_2-Au was unable to generate O_2^-. These results indicate that TiO_2-Au heterostructures exhibited higher ROS quantum yield than TiO_2. It can be ascribed to that Au nanoclusters as electron sinks modified the bandgap structures of TiO_2, thereby enhancing the separation efficiency of e^-/h^+ pairs in SDT process.[20,31] As shown in Figure 2F,

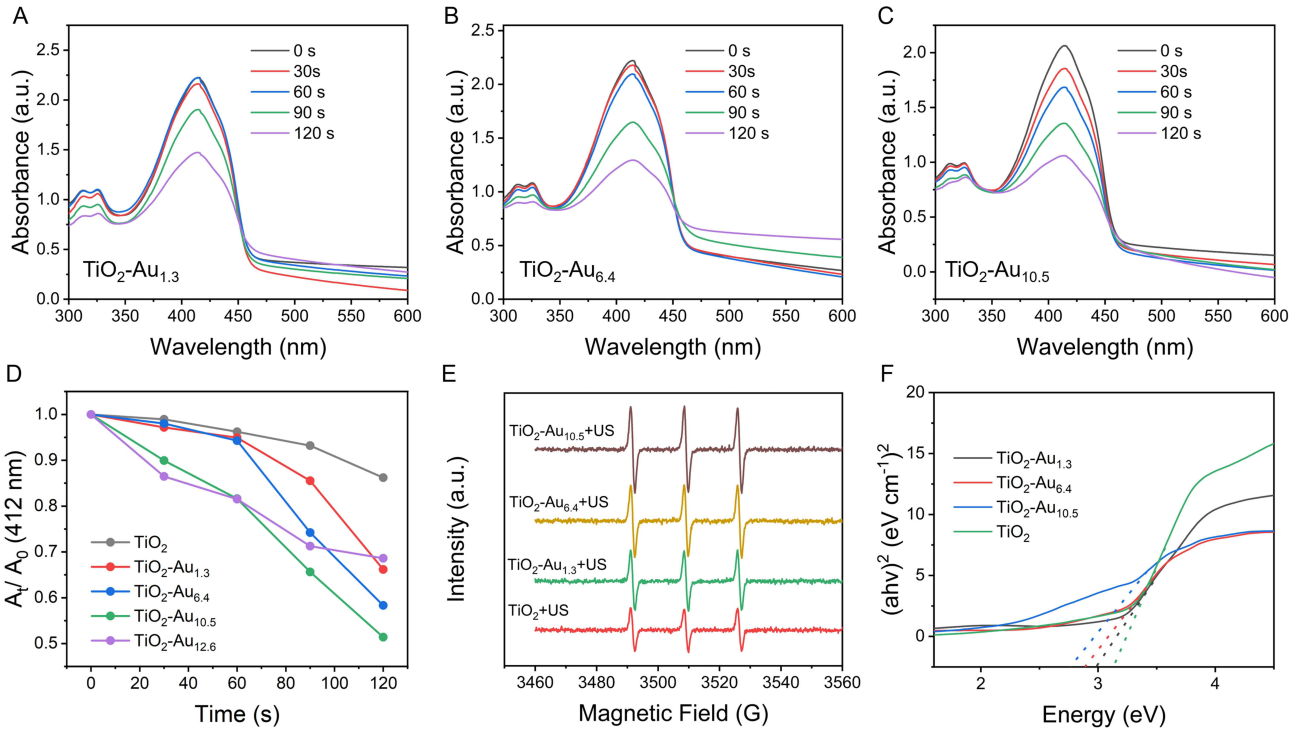

Figure 2 Physiochemical properties of synthesized TiO_2-Au. (**A–C**) Absorption decay of DPBF probe under US irradiation at various time intervals in the presence of TiO_2-Au. (**D**) Comparison of DPBF absorbance decay over treatment period. (**E**) ESR spectrum of 2,2,6,6-tetramethylpiperidine (TEMP)/$^1O_2$ adducts in pristine TiO_2 and TiO_2-Au groups. (**F**) The respective UV-vis diffuse reflectance spectra of TiO_2 and TiO_2-Au.

the bandgap of TiO_2 was decreased from 3.2 eV to 2.8 eV after Au nanoclusters deposition. Additionally, the presence of Au clusters significantly improved light absorption in the 450–800 nm range compared to pristine TiO_2 (Figure S10), which corresponds well with the emission spectrum of sonoluminescence in aqueous media. Consequently, both improved e^-/h^+ separation and enhanced light absorption lead to a substantial increase ROS production in TiO_2-Au heterostructure.

The intracellular ROS levels and therapeutic efficiency of TiO_2-Au in vitro were investigated using breast cancer 4T1 cells. Flow cytometry analysis was conducted to assess the ROS levels using DCFH-DA as probes (Figure 3A). It was found that the fluorescence intensity of DCFH-DA probes increased as Au content in TiO_2-Au increased, indicating that TiO_2-Au can effectively produce $^1O_2$ under US irradiation within the cellular environment. Notably, the fluorescence intensity in the TiO_2-$Au_{10.5}$ + US group was 4.25-fold higher than that in TiO_2 + US group, demonstrating elevated ROS levels. Next, the apoptosis rate of treated 4T1 cells were assessed using flow cytometry (Figure 3B), revealing a correlation between increased ROS levels and higher apoptosis rates. The TiO_2-$Au_{10.5}$ + US group exhibited an apoptosis rate of 48.2%, which was 4.7-fold higher than the TiO_2 + US group. The differentiation between live and dead cells were further established through the co-staining of Calcein acetoxymethyl ester and propidium iodide (Calcein-AM /PI). As shown in Figure 3C, the TiO_2-$Au_{10.5}$ + US group exhibited significantly stronger red fluorescence, indicating a higher proportion of dead cells, while the other groups showed intense green fluorescence, suggesting that most cells remained alive. Without US irradiation, no significant cytotoxic effects were observed, even at high concentrations of TiO_2 and TiO_2-$Au_{10.5}$ (up to 300 μg/mL, Figures 3D and S11). However, upon US exposure, the cell mortality rate in the TiO_2-$Au_{10.5}$ nanoparticle group exceeded 60%, indicating a pronounced cytotoxic effect compared to the TiO_2 group alone, suggesting a synergy between the gold doping (Au) and ultrasound exposure that enhances the therapeutic effect.

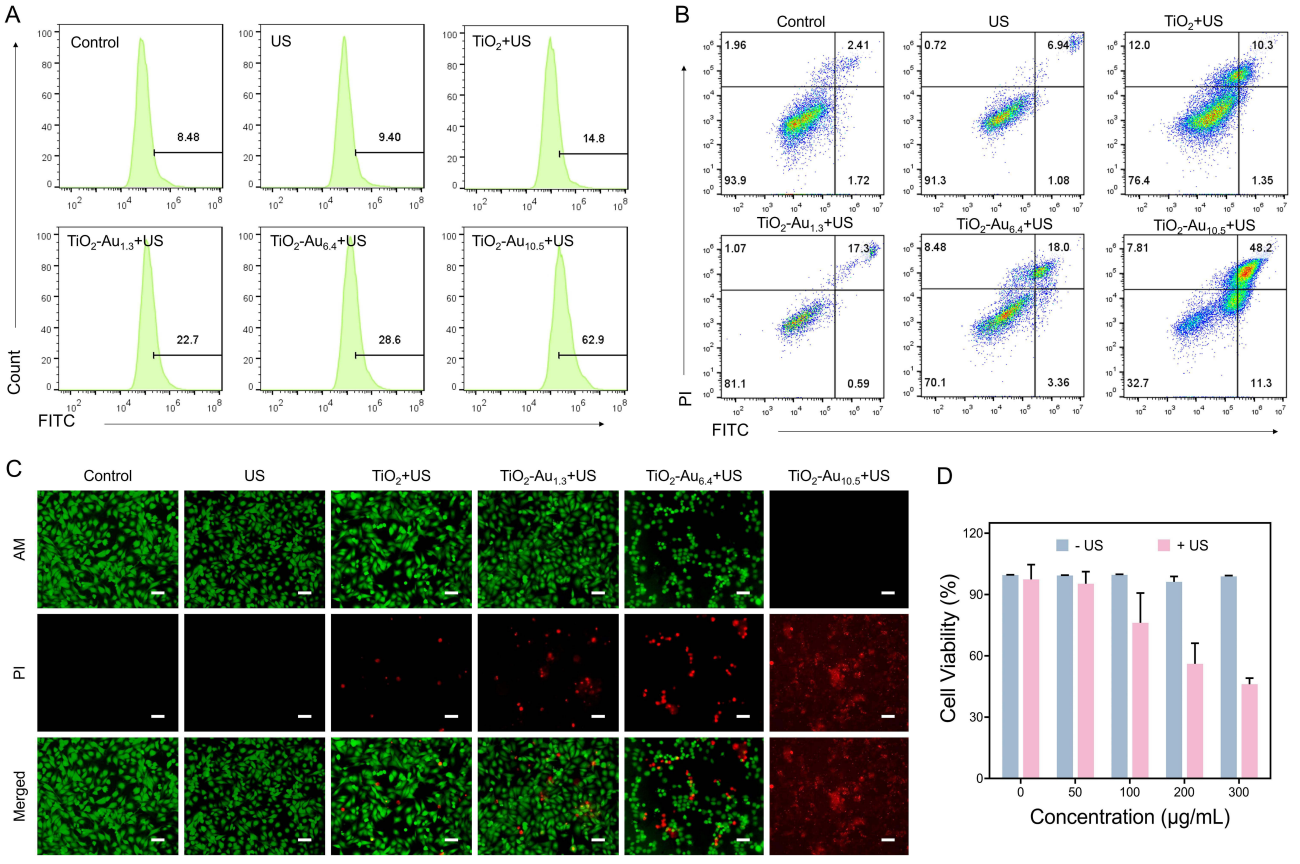

Figure 3 Detection of ROS levels and cell viability. (**A**) Flow-cytometry analysis of 4T1 cells stained with DCFH-DA. (**B**) Flow-cytometry assay to evaluate the apoptosis of 4T1 cells after various treatments. (**C**) The fluorescence imaging of tumor cells treated by sonosensitizers, which was stained by Calcein-AM/PI. (**D**) Cell viability of 4T1 cells with or without US irradiation power and concentrations. The embedded scale bars correspond to 50 μm.

https://doi.org/10.2147/IJN.S516314

Building on the promising in vitro antitumor results, we further assessed the in vivo efficacy of TiO_2-Au-mediated SDT in 4T1 tumor-bearing BALB/c mice. The mice were randomly assigned to three groups (n=4 per group): Control (PBS), US and TiO_2-$Au_{10.5}$+US. As illustrated in Figure 4A, treatments were administered over a 14-day period, with tumor size and weight recorded every two days (Figure 4B and C and S12). While the US and TiO_2-$Au_{10.5}$ groups exhibited minimal tumor inhibition compared to the control, the combined TiO_2-$Au_{10.5}$+US treatment markedly suppressed tumor growth, achieving tumor growth inhibition (TGI) indices of 76.9% based on tumor volume (Figure 4D–F). Histological analysis of tumor tissues via hematoxylin and eosin (H&E) staining revealed substantial tissue damage in the TiO_2-$Au_{10.5}$+US group (Figure 4G), whereas the Control, US, and TiO_2-$Au_{10.5}$ groups displayed normal cell morphology with intact membrane and nuclear structures. These findings underscore the significant tumor-suppressive effect of TiO_2-$Au_{10.5}$+US, attributable to enhanced SDT.

The biocompatibility of TiO_2-$Au_{10.5}$ sonosensitizers was thoroughly evaluated. As shown in Figures 5A and S13, even at a high concentration of 200 μg/mL, no hemolysis was observed, demonstrating excellent hemocompatibility. Furthermore, the results of biochemical analysis indicated that crucial indicators of liver and kidney function, including ALT (alanine aminotransferase), AST (aspartate aminotransferase), ALP (alkaline phosphatase), BUN

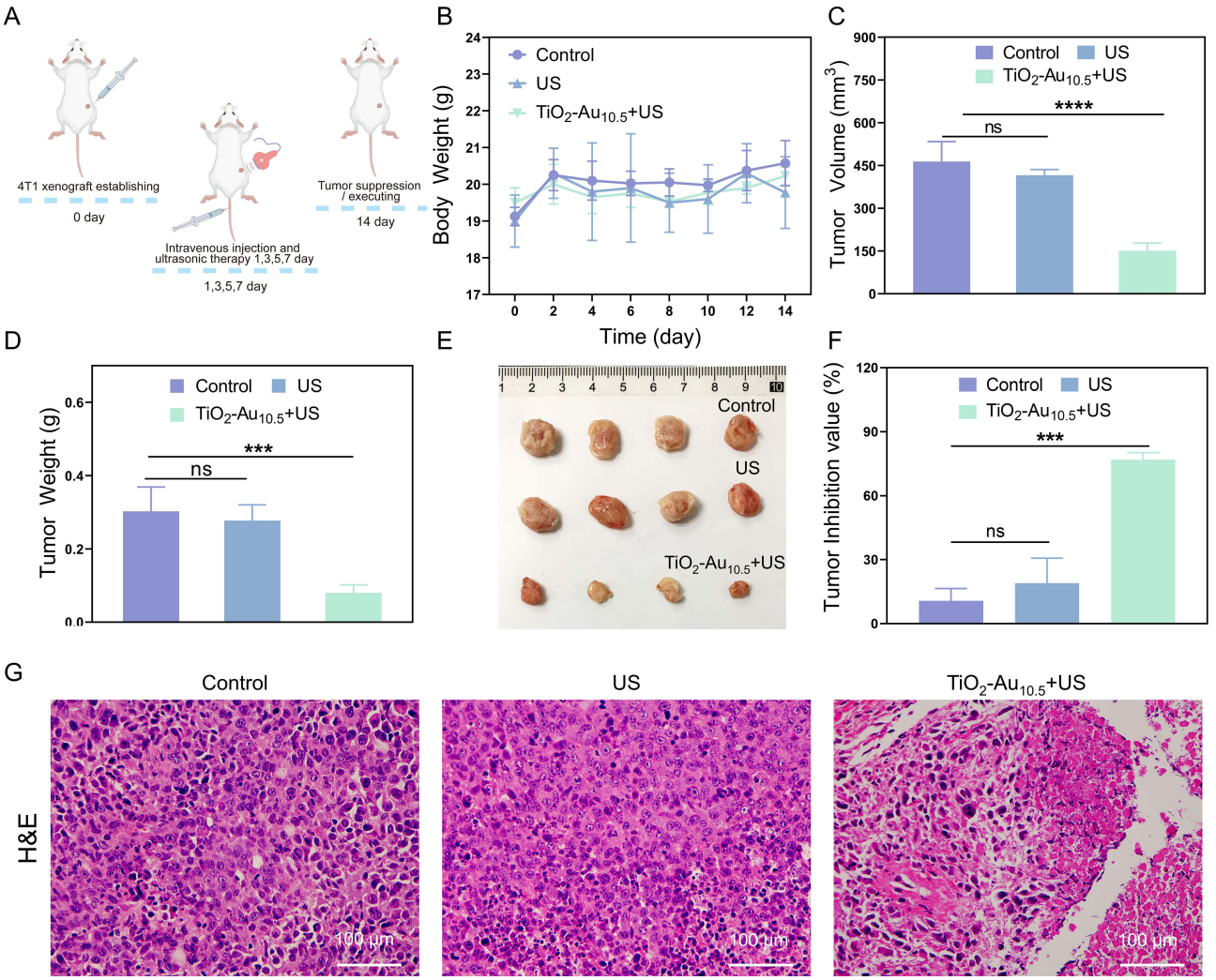

Figure 4 In vivo antitumor performance. (**A**) Schematic illustration of therapeutic protocol. (**B**) The change of body weight after various treatments. (**C**) The comparison of tumor volume after various treatments on day 14. (**D**) The comparison of tumor weight after various treatments on day 14. (**E**) Photographs of excised tumors on day 14 (n = 4). (**F**) The change of tumor growth inhibition rate after various treatments. (**G**) H&E slice images of tumors after various treatments. The embedded scale bars correspond to 100 μm. Data is shown as mean ± SD, P-values were calculated by using one-way ANOVA with the Tukey's multiple comparison analysis: ***P < 0.001, ****P < 0.0001.

Abbreviation: ns, no significant difference.

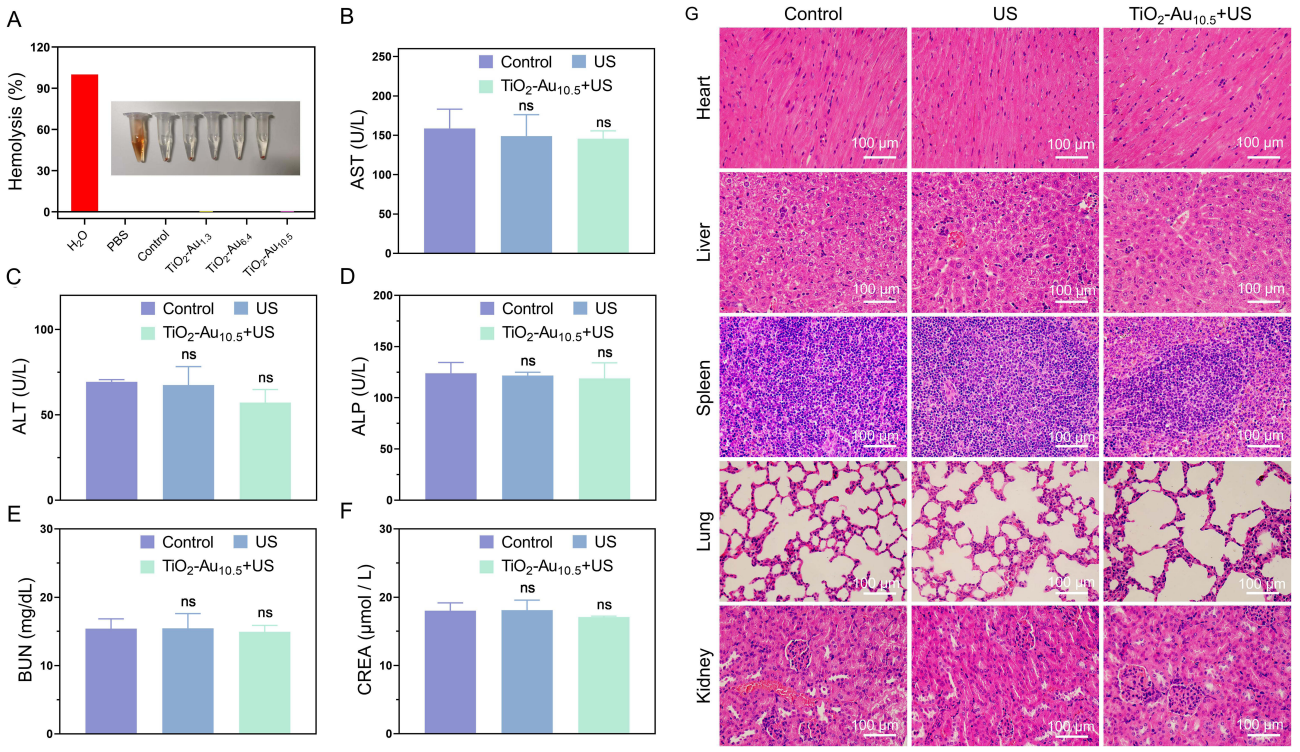

Figure 5 Biosafety assessment of TiO_2-$Au_{10.5}$+ US. (**A**) The hemolysis analysis of TiO_2-Au. (**B–F**) Blood biochemical test results of mice with various treatments (TiO_2-$Au_{10.5}$+US, US or PBS): AST, ALT, ALP, BUN, and CREA. The biochemical reference values of BALB/C mice are as follows: AST: 36.31–235.48 U/L, ALT: 10.06–96.47 U/L, ALP: 22.52–474.35 U/L, BUN: 10.81–34.74 mg/dL, and CREA: 10.91–85.09 μmol/L. (**G**) H&E staining of tissues from major organs of mice after various treatment. The embedded scale bars correspond to 100 μm. Data is shown as mean ± SD, P-values were calculated by using one-way ANOVA with the Tukey's multiple comparison analysis. **Abbreviation**: ns, no significant difference.

(blood urea nitrogen), and CREA (creatinine) levels, remained within the normal range across all groups subjected to treatment (Figures 5B–F), indicating minimal risk of inflammation, hepatotoxicity, or nephrotoxicity. Furthermore, histological examination of major organs via H&E staining showed no significant tissue damage (Figure 5G), confirming the good biocompatibility of TiO_2-$Au_{10.5}$. Additionally, body weight increased steadily across all groups during the treatment period (Figure 4B), suggesting minimal toxicity or adverse effects from the TiO_2-$Au_{10.5}$ treatment.

Conclusions

In summary, we investigated the utilization of Au nanocluster-modified TiO_2 nanosheets (TiO_2-Au) to enhance sonodynamic therapy (SDT) for breast cancer. The addition of Au clusters to TiO_2 led to a notable decrease in its bandgap, which consequently promoted the separation of electron-hole pairs and enhanced the generation of reactive oxygen species (ROS). In vitro experiments revealed that when activated by ultrasound (US), TiO_2-$Au_{10.5}$ exhibited a significant augmentation in cell apoptosis compared to pristine TiO_2. Furthermore, in vivo studies provided compelling evidence showcasing substantial tumor suppression and high tumor growth inhibition (TGI) in mice treated with TiO_2-$Au_{10.5}$ + US, Biocompatibility studies, including hemolysis assays, histological analysis, and biochemical assessments, showed no significant toxicity. These findings strongly suggest that TiO_2-$Au_{10.5}$ holds great promise as an effective and biocompatible sonosensitizer for cancer therapy.

Data Sharing Statement

The data that support the findings of this study are available from the corresponding author, [Weiqing Zhang], upon reasonable request.

https://doi.org/10.2147/IJN.S516314

Author Contributions

All authors made a significant contribution to the work reported, whether that is in the conception, study design, execution, acquisition of data, analysis and interpretation, or in all these areas; took part in drafting, revising or critically reviewing the article; gave final approval of the version to be published; have agreed on the journal to which the article has been submitted; and agree to be accountable for all aspects of the work.

Funding

The authors appreciate financial supports from the Joint Project on Regional High-Incidence Diseases Research of Guangxi Natural Science Foundation (2024GXNSFAA010157). Advanced Innovation Teams and Xinghu Scholars Program of Guangxi Medical University, and start-up funding for high-level talents from Guangxi Medical University Cancer Hospital.

Disclosure

The authors declare that they have no known competing financial interests or personal relationships that could have appeared to influence the work reported in this paper.

References

1. Bray F, Laversanne M, Sung HYA, et al. Global cancer statistics 2022: GLOBOCAN estimates of incidence and mortality worldwide for 36 cancers in 185 countries. *CA-Cancer J Clin*. 2024;74(3):229–263. doi:10.3322/caac.21834
2. Guo XL, Yang ND, Ji WH, et al. Mito-bomb: targeting mitochondria for cancer therapy. *Adv Mater*. 2021;33(43):e2007778. doi:10.1002/adma.202007778
3. Liang S, Deng XR, Ma PA, Cheng ZY, Lin J. Recent advances in nanomaterial-assisted combinational sonodynamic cancer therapy. *Adv Mater*. 2020;32(47)::e2003214. doi:10.1002/adma.202003214
4. McHale AP, Callan JF, Nomikou N, Fowley C, Callan B. Sonodynamic therapy: concept, mechanism and application to cancer treatment. *Ther Ultrasound*. 2016;880:429–450.
5. Wang PH, Chen J, Zhong RM, et al. Recent advances of ultrasound-responsive nanosystems in tumor immunotherapy. *Eur J Pharm Biopharm*. 2024;198:114246. doi:10.1016/j.ejpb.2024.114246
6. Bai S, Yang NL, Wang XW, et al. Ultrasmall iron-doped titanium oxide nanodots for enhanced sonodynamic and chemodynamic cancer therapy. *ACS Nano*. 2020;14(11):15119–15130. doi:10.1021/acsnano.0c05235
7. Chen P, Zhang P, Shah NH, Cui Y, Wang Y. A comprehensive review of inorganic sonosensitizers for sonodynamic therapy. *Int J Mol Sci*. 2023;24(15):12001. doi:10.3390/ijms241512001
8. Wei LN, Wang ZY, Lu XX, et al. Interfacial strong interaction-enabling cascade nanozymes for apoptosis-ferroptosis synergistic therapy. *J Colloid Interface Sci*. 2024;653:20–29. doi:10.1016/j.jcis.2023.09.036
9. Chen QQ, Zhang M, Huang H, et al. Single atom-doped nanosonosensitizers for mutually optimized sono/chemo-nanodynamic therapy of triple negative breast cancer. *Adv Sci*. 2023;10(6):e2206244. doi:10.1002/advs.202206244
10. Wen SW, Zhang WY, Yang JL, Zhou ZJ, Xiang Q, Dong HF. Ternary Bi_2WO_6/TiO_2-Pt heterojunction sonosensitizers for boosting sonodynamic therapy. *ACS Nano*. 2024;18(34):23672–23683. doi:10.1021/acsnano.4c08236
11. Perota G, Zahraie N, Vais RD, Zare MH, Sattarahmady N. Au/TiO_2 nanocomposite as a triple-sensitizer for 808 and 650 nm phototherapy and sonotherapy: synergistic therapy of melanoma cancer in vitro. *J Drug Deliv Sci Technol*. 2022;76:103787. doi:10.1016/j.jddst.2022.103787
12. Zlotver I, Sosnik A. Glucosylated hybrid TiO_2/polymer nanomaterials for actively targeted sonodynamic therapy of cancer. *Small*. 2023;20(4):e2305475. doi:10.1002/smll.202305475
13. Wang XW, Zhong XY, Bai LX, et al. Ultrafine titanium monoxide (TiO_{1+x}) nanorods for enhanced sonodynamic therapy. *J Am Chem Soc*. 2020;142(14):6527–6537. doi:10.1021/jacs.9b10228
14. Liu W, Shao RR, Guo LY, et al. Precise design of TiO_2@CoO_x heterostructure via atomic layer deposition for synergistic sono-chemodynamic oncotherapy. *Adv Sci*. 2024;11(14):e2304046. doi:10.1002/advs.202304046
15. Li GL, Wu SC, Liu JG, Wang KY, Chen XY, Liu HX. Narrow bandgap schottky heterojunction sonosensitizer with high electron-hole separation boosted sonodynamic therapy in bladder cancer. *Adv Mater*. 2024;36(26):e2401252. doi:10.1002/adma.202401252
16. Qiao X, Xue L, Huang H, Dai X, Chen Y, Ding H. Engineering defected 2D Pd/H-TiO_2 nanosonosensitizers for hypoxia alleviation and enhanced sono-chemodynamic cancer nanotherapy. *J Nanobiotechnology*. 2022;20(1):186. doi:10.1186/s12951-022-01398-6
17. Lu XX, Qiao K, Shaik F, et al. Evoking robust immunogenic cell death by synergistic sonodynamic therapy and glucose depletion using Au clusters/single atoms modified TiO_2 nanosheets. *Nano Res*. 2023;16(7):9730–9742. doi:10.1007/s12274-023-5562-9
18. Zhao YM, Liu JH, He MT, et al. Platinum-itania schottky junction as nanosonosensitizer, glucose scavenger, and tumor microenvironment-modulator for promoted cancer treatment. *ACS Nano*. 2022;16(8):12118–12133. doi:10.1021/acsnano.2c02540
19. Liang S, Deng XR, Xu GY, et al. A novel Pt-TiO_2 heterostructure with oxygen-deficient layer as bilaterally enhanced sonosensitizer for synergistic chemo-sonodynamic cancer therapy. *Adv Funct Mater*. 2020;30(13):1908598. doi:10.1002/adfm.201908598
20. Park SH, Kim S, Park JW, Kim S, Cha W, Lee J. In-situ and wavelength-dependent photocatalytic strain evolution of a single Au nanoparticle on a TiO_2 film. *Nat Commun*. 2024;15(1):5416. doi:10.1038/s41467-024-49862-1
21. Wang D, Zhang J-T. Metal-based inorganic nanocrystals for biological sonodynamic therapy applications: recent progress and perspectives. *Rare Met*. 2023;43(2):413–430. doi:10.1007/s12598-023-02450-6

22. Elahi N, Kamali M, Baghersad MH. Recent biomedical applications of gold nanoparticles: a review. *Talanta*. 2018;184:537–556. doi:10.1016/j.talanta.2018.02.088
23. Yang YQ, Wang XW, Qian HS, Cheng L. Titanium-based sonosensitizers for sonodynamic cancer therapy, Appl. *Mater Today*. 2021;25:101215.
24. Qu J, Wang Y, Mu X, et al. Determination of crystallographic orientation and exposed facets of titanium oxide nanocrystals. *Adv Mater*. 2022;34 (37):2203320. doi:10.1002/adma.202203320
25. Ning S, Dai X, Tang W, et al. Cancer cell membrane-coated C-TiO_2 hollow nanoshells for combined sonodynamic and hypoxia-activated chemotherapy. *Acta Biomater*. 2022;152:562–574. doi:10.1016/j.actbio.2022.08.067
26. Bharti B, Kumar S, Lee H-N, Kumar R. Formation of oxygen vacancies and Ti^{3+} state in TiO_2 thin film and enhanced optical properties by air plasma treatment, Sci. *Rep*. 2016;6(1):32355.
27. Xu FY, Meng K, Cheng B, Wang SY, Xu JS, Yu JG. Unique S-scheme heterojunctions in self-assembled TiO_2/$CsPbBr_3$ hybrids for CO_2 photoreduction. *Nat Commun*. 2020;11(1):4613. doi:10.1038/s41467-020-18350-7
28. Zhang Y, Liu JX, Qian K, et al. Structure sensitivity of Au-TiO_2 strong metal-support interactions. *Angew Chem Int Ed*. 2021;60(21):12074–12081. doi:10.1002/anie.202101928
29. Amin MO, Al-Hetlani E. Development of efficient saldi substrate based on Au-TiO_2 nanohybrids for environmental and forensic detection of dyes and NSAIDs. *Talanta*. 2021;233:122530. doi:10.1016/j.talanta.2021.122530
30. Entradas T, Waldron S, Volk M. The detection sensitivity of commonly used singlet oxygen probes in aqueous environments. *J Photochem Photobiol B: Biol*. 2020;204:111787. doi:10.1016/j.jphotobiol.2020.111787
31. Cao XS, Li MX, Liu QY, Zhao JJ, Lu XH, Wang JW. Inorganic sonosensitizers for sonodynamic therapy in cancer treatment. *Small*. 2023;19(42): e2303195. doi:10.1002/smll.202303195